

# DETECTION OF DARK MATTER CONCENTRATIONS IN THE FIELD OF CL 1604+4304 FROM WEAK LENSING ANALYSIS

KEIICHI UMETSU AND TOSHIFUMI FUTAMASE  
 Astronomical Institute, Tohoku University, Sendai 980-8578, Japan  
 keiichi@astr.tohoku.ac.jp, tof@astr.tohoku.ac.jp  
*Accepted for publication in The Astrophysical Journal Letters*

## ABSTRACT

We present a weak-lensing analysis of a region around the galaxy cluster Cl 1604+4304 ( $z = 0.897$ ) on the basis of the deep observations with the *Hubble Space Telescope* (*HST*)/Wide Field Planetary Camera 2 (WFPC2). We apply a variant of Schneider's aperture mass technique to the observed WFPC2 field and obtain the distribution of weak-lensing signal-to-noise ratio (S/N) within the field. The resulting S/N map reveals a clear pronounced peak located about  $1'.7$  ( $850h_{50}^{-1}$  kpc at  $z = 0.897$ ) southwest of the second peak associated with the optical cluster center determined from the dynamical analysis of Postman et al. A non-linear finite-field inversion method has been used to reconstruct the projected mass distribution from the observed shear field. The reconstructed mass map shows a super-critical feature at the location of the S/N peak as well as in the cluster central region. Assuming the redshift distribution of field galaxies, we obtain the total mass in the observed field to be  $1.0 \times 10^{15} h_{50}^{-1} M_{\odot}$  for  $\langle z \rangle = 1.0$ . The estimated mass within a circular aperture of radius  $280h_{50}^{-1}$  kpc centered on the dark clump is  $2.4 \times 10^{14} h_{50}^{-1} M_{\odot}$ . We have confirmed the existence of the 'dark' mass concentration from another deep *HST* observation with a slightly different ( $\sim 20''$ ) pointing.

*Subject headings:* cosmology: observations — dark matter — galaxies: clusters: individual (Cl 1604+4304) — gravitational lensing

## 1. INTRODUCTION

Weak shear fields of high-redshift galaxies are promising, efficient tools to investigate the mass distribution on cluster-supercluster scales (Kaiser & Squires 1993; Lupino & Kaiser 1997; Kaiser et al. 1998; Bartelmann & Schneider 2000) and provide a unique mean to detect dark mass concentrations (Schneider 1996; Erben et al. 2000). Wide-field weak-lensing surveys of projected mass overdensities can probe the statistical clustering properties and underlying cosmology (Bahcall et al. 1999).

Recent observations have revealed the existence of a supercluster at a high redshift of  $z \approx 0.9$  (Lubin et al. 2000). This supercluster contains two massive galaxy clusters, Cl 1604+4304 at  $z = 0.897$  and Cl 1604+4321 at  $z = 0.924$ . The two clusters are separated by  $17'$  on the sky, corresponding to a projected separation of  $\sim 9h_{50}^{-1}$  Mpc. Cl 1604+4304 is located at  $(\alpha_{J2000}, \delta_{J2000}) = (16^{\text{h}} 04^{\text{m}} 19.5^{\text{s}}, +43^{\circ} 04' 33''.9)$  and one of the optically-selected high-redshift cluster candidates studied by Oke, Postman, & Lubin (1998). Postman, Lubin, & Oke (1998) presented a detailed photometric and spectroscopic survey of the cluster and obtained a velocity dispersion of  $1226 \text{ km s}^{-1}$  and a dynamical mass estimate of  $6.2 \times 10^{15} h_{50}^{-1} M_{\odot}$ .

In this Letter, we present a weak lensing analysis of the Cl 1604+4304 field on the basis of deep images taken with the *Hubble Space Telescope* (*HST*)/Wide Field Planetary Camera 2 (WFPC2). We shall mainly describe the weak-lensing signal-to-noise ratio (S/N) analysis of the observed field; the details of the mass reconstruction procedure will be present elsewhere. Throughout this Letter, we adopt  $\Omega_0 = 1$ ,  $\Omega_{\Lambda} = 0$ , and  $H_0 = 50h_{50} \text{ km s}^{-1} \text{ Mpc}^{-1}$ ;  $1'$  on the sky corresponds to  $0.52h_{50}^{-1}$  Mpc at the cluster redshift.

## 2. OBSERVATIONS AND DATA REDUCTION

The cluster Cl 1604+4304 field was observed in 1994 and 1995 using the WFPC2 camera with the F814W filter on board the *HST* (P.I.: J. Westphal; proposal 5234). We retrieved the calibrated data for Cl 1604+4304 field from the *HST* archive. Both the 1994 and 1995 observations have the same total exposure time of 32 ksec, consisting of 16 single orbits of 2 ksec. The 1995 pointing covers the central region of Cl 1604+4304 (Lubin et al. 1998), while the 1994 pointing is about  $20''$  offset ( $\Delta X \simeq 0'.1$ ,  $\Delta Y \simeq 18''.2$ ) from the 1995 pointing. For this reason, Lubin et al. (1998) discarded the 1994 data from their analysis. We analyze both the 1994 and 1995 data separately. For each observation, the data were shifted and combined into the final frame to remove cosmic rays using the IRAF/STSDAS task CR-REJ. The PC chip was discarded from our analysis because of its brighter isophotal limit, so that the final frame for each observation consists of three WFC chips. The side length of the WFPC2 field is about  $2'.5$  ( $1.26h_{50}^{-1}$  Mpc at  $z = 0.897$ ).

We use the SExtractor package (Bertin & Arnouts 1996) for the object detection, photometry, and measurement of image shapes. We extract all objects with isophotal areas larger than 12 pixels ( $0''.0996 \text{ pixel}^{-1}$ ) above  $2\sigma \text{ pixel}^{-1}$  of the local sky level. We calculate the total magnitudes  $I_{814W}$  in STMAG system for each object using MAG\_BEST parameters in SExtractor. The corresponding detection thresholds for the 1994 and 1995 data are  $\mu_{814W} = 26.2$  and  $26.5 \text{ mag arcsec}^{-2}$ , respectively. We measure the quadrupole moments  $Q_{ij} = \int d^2\theta \theta_i \theta_j I(\vec{\theta}) / \int d^2\theta I$  of the surface brightness  $I(\vec{\theta})$  for each object, where the center of light is chosen as the coordinate origin. From  $\{Q_{ij}\}$ , we construct the image

ellipticity  $\epsilon_i = (Q_{11} - Q_{22}, 2Q_{12})/(\text{Tr}(Q) + 2(\det Q)^{1/2})$  ( $i = 1, 2$ ). To construct catalogs of faint galaxies, we refer to the following SExtractor output parameters: We exclude objects with FLAGS (extraction flags)  $\geq 1$  from our analysis. We make star/galaxy separation using the CLASS\_STAR parameter (stellarity index) and keep the objects with CLASS\_STAR  $\leq 0.2$  as faint galaxy candidates. Objects with FWHM\_IMAGE (FWHM profile from a Gaussian fit to the core)  $< 4$  pixels are excluded since image shapes of extremely small objects relative to the pixel scale may be affected by the anisotropic PSF. Finally, all objects with  $I_{814W} \in (25.5, 27.5)$  are selected as background galaxy candidates. This detection and selection procedure leads to the final catalogs with total galaxy numbers of  $N_g = 200$  and  $241$ , corresponding number densities of  $n_g = 45.8$  and  $56.8 \text{ arcmin}^{-2}$ , for the 1994 and 1995 data, respectively.

### 3. WEAK LENSING ANALYSIS

#### 3.1. Strategy

Our first aim is to obtain the distribution of weak-lensing S/N in the data field. Then, the high peaks in the S/N maps can be identified as clusters or mass overdensities. To do this, we make use of a variant of aperture mass statistics. The statistics rely on the fact that the shear  $\gamma = (\gamma_1, \gamma_2)$  and the convergence  $\kappa := \Sigma/\Sigma_{\text{cr}}$  are related to each other through  $\vec{\nabla}\kappa = \hat{D}\gamma \equiv \vec{u}_\gamma$ , where  $\Sigma$  is the surface mass density of the deflector,  $\Sigma_{\text{cr}} = (c^2/4\pi G)D_s/D_d D_{\text{ds}}$  is the critical surface mass density, and  $\hat{D} = \{\hat{D}_{ij}\}$  ( $i, j = 1, 2$ ) is a differential operator defined by

$$\hat{D} = \begin{pmatrix} \partial/\partial\theta_1 & \partial/\partial\theta_2 \\ -\partial/\partial\theta_2 & \partial/\partial\theta_1 \end{pmatrix} \quad (1)$$

(Kaiser 1995). Since  $\vec{u}_\gamma$  is the gradient of  $\kappa$ , operating  $\hat{D}$  further on  $\vec{u}_\gamma$  yields

$$(\Delta\kappa, 0) = \hat{D}^2\gamma = \hat{D}\vec{u}_\gamma = (\text{div}\vec{u}_\gamma, \text{rot}\vec{u}_\gamma). \quad (2)$$

In weak lensing limit ( $\kappa \ll 1$  and  $|\gamma| \ll 1$ ), the expectation value of the image ellipticity,  $E[\epsilon(\vec{\theta})]$ , is the shear  $\gamma(\vec{\theta})$ . In practice, however, background sources have intrinsic ellipticities  $\epsilon_{(s)}$ , so that weak lensing analysis involves the smoothing procedure to reduce the noise. We denote the smoothed fields by angular brackets  $\langle \rangle$ : e.g.,  $\langle \kappa \rangle = \int d^2\theta' W(|\vec{\theta} - \vec{\theta}'|; \vartheta) \kappa(\vec{\theta}')$ , where  $W(\theta; \vartheta)$  is a smooth, continuous window function with a characteristic scale of  $\vartheta$ . Because of the commutativity between smoothing and the mass reconstruction (Van Waerbeke 2000), the smoothed quantities  $\langle \kappa \rangle$  and  $\langle \gamma \rangle$  satisfies the same relations as those between  $\kappa$  and  $\gamma$ :  $\vec{\nabla}\langle \kappa \rangle = \hat{D}\langle \gamma \rangle \equiv \vec{u}_{\langle \gamma \rangle}$ ;  $(\Delta\langle \kappa \rangle, 0) = \hat{D}^2\langle \gamma \rangle = \hat{D}\vec{u}_{\langle \gamma \rangle} = (\text{div}\vec{u}_{\langle \gamma \rangle}, \text{rot}\vec{u}_{\langle \gamma \rangle})$ . The Laplacian of  $\langle \kappa \rangle$ , i.e.  $\text{div}\vec{u}_{\langle \gamma \rangle}$ , is just the convergence convolved with the compensated filter function  $\Delta W$ , and hence equivalent to the aperture mass. Defining  $\vec{u}_{\langle \epsilon \rangle} := \hat{D}\langle \epsilon \rangle$ , we see that the observable  $\text{div}\vec{u}_{\langle \epsilon \rangle}$  traces the distribution of  $\Sigma$  in the limit of weak lensing, as pointed out by Luppino & Kaiser (1997). On the other hand,  $\text{rot}\vec{u}_{\langle \epsilon \rangle}$  measures the ‘pure’ noise. A discretized estimator for  $\hat{D}\vec{u}_{\langle \gamma \rangle}$  is given by  $\hat{D}\vec{u}_{\langle \epsilon \rangle} = (\text{div}\vec{u}_{\langle \epsilon \rangle}, \text{rot}\vec{u}_{\langle \epsilon \rangle}) = -n_g^{-1} \sum_{m=1}^{N_g} p(|\vec{\theta} -$

$\vec{\theta}_m|; \vartheta) [\epsilon_t(\vec{\theta}_m; \vec{\theta}), \epsilon_r(\vec{\theta}_m; \vec{\theta})]$ , where  $\epsilon_t$  and  $\epsilon_r$  are the tangential and the radial components of the image ellipticity  $\epsilon = \epsilon_1 + i\epsilon_2$  defined by  $\epsilon_t(\vec{\theta}; \vec{\theta}_0) := -\Re[\epsilon(\vec{\theta})e^{-2i\phi}]$  and  $\epsilon_r(\vec{\theta}; \vec{\theta}_0) := -\Im[\epsilon(\vec{\theta})e^{-2i\phi}]$  with  $\phi = \text{Arg}(\vec{\theta} - \vec{\theta}_0)$  and  $p(\theta; \vartheta) = W''(\theta; \vartheta) - W'(\theta; \vartheta)/\theta$ . The noise properties of  $\hat{D}^2\langle \epsilon \rangle$  due to the intrinsic source ellipticities are contained in the covariant matrix  $\sigma_{ij}^2 := E[\hat{D}^2\langle \epsilon^{(s)} \rangle \hat{D}^2\langle \epsilon^{(s)} \rangle]_{ij}$ :

$$\sigma_{ij}^2(\vec{\theta}) = \delta_{ij} \frac{\sigma_\epsilon^2}{2n_g^2} \sum_{m=1}^{N_g} p^2(|\vec{\theta} - \vec{\theta}_m|; \vartheta) \equiv \delta_{ij} \sigma^2(\vec{\theta}), \quad (3)$$

where  $\sigma_\epsilon$  is the dispersion of the intrinsic source ellipticities and we have assumed  $E[\epsilon^{(s)}(\vec{\theta}_m)\epsilon^{(s)}(\vec{\theta}_n)]_{ij} = \delta_{ij}\delta_{mn}\sigma_\epsilon^2/2$ . The Kronecker delta  $\delta_{ij}$  in equation (3) ensures that the dispersions of  $\text{div}\vec{u}_{\langle \epsilon \rangle}$  and  $\text{rot}\vec{u}_{\langle \epsilon \rangle}$  are the same and that the two fields are statistically uncorrelated. The local weak-lensing S/N  $\nu(\vec{\theta})$  at position  $\vec{\theta}$  is then defined by

$$\nu(\vec{\theta}) := -\frac{\text{div}\vec{u}_{\langle \epsilon \rangle}(\vec{\theta})}{\sigma(\vec{\theta})} = \frac{\sqrt{2} \sum_m p(|\vec{\theta} - \vec{\theta}_m|; \vartheta) \epsilon_t(\vec{\theta}_m; \vec{\theta})}{\sigma_\epsilon \sqrt{\sum_m p^2(|\vec{\theta} - \vec{\theta}_m|; \vartheta)}}. \quad (4)$$

The resulting formula (eq. [4]) is equivalent to the one derived by Schneider (1996) using aperture mass statistics. In the present Letter, we use a Gaussian window function of the form  $W_G(\theta; \vartheta) = \exp(-\theta^2/\vartheta^2)/\pi\vartheta^2$ , in which case  $p(\theta; \vartheta) = 4(\theta/\vartheta)^2 \exp(-\theta^2/\vartheta^2)/\pi\vartheta^4 \equiv p_G(\theta; \vartheta)$ ;  $p_G(\theta; \vartheta)$  has its maximum at  $\theta = \vartheta$  and falls off rapidly at  $\theta > \vartheta$ . These statistics can be applied to the strong-lensing regime (e.g., cluster central region), because the contribution of image ellipticities to the aperture mass comes mainly from galaxies within an annulus at radius  $\vartheta$  and thus we can avoid the strong lensing regime. For each independent *HST* observation, we perform a local S/N analysis using equation (4).

To obtain the projected mass distribution, we perform a mass reconstruction to the *HST*/WFC field. Taking into account the high redshift ( $z = 0.897$ ) of Cl 1604+4304 and small field-of-view ( $2'5$  on a side) of the *HST*/WFC field, we adopt a non-linear finite-field inversion method developed by Seitz & Schneider (1997), which takes account of the source redshift distribution. Since little is known about the redshift distribution of field galaxies, we assume a source redshift distribution of the form  $p_z(z) = \beta z^2 \exp[-(z/z_0)^\beta]/\Gamma(3/\beta)z_0^3$  (Brainerd, Blandford, & Smaili 1996), in which case the mean redshift  $\langle z \rangle$  is given by  $\langle z \rangle = z_0\Gamma(4/\beta)/\Gamma(3/\beta)$ . In the present Letter, we consider only the case  $(\langle z \rangle, \beta) = (1.0, 1.0)$ .

Once a smoothed ellipticity field  $\langle \epsilon \rangle(\vec{\theta})$  is obtained from the observed image ellipticities, a convergence map can be obtained through the integral equation

$$\kappa_\infty(\vec{\theta}) - \bar{\kappa}_\infty = \int_{\mathcal{U}} d^2\theta' \vec{H}(\vec{\theta}, \vec{\theta}') \cdot \vec{u}_{\gamma_\infty}(\vec{\theta}'), \quad (5)$$

where quantities with  $\infty$ -subscript represent the values for sources at infinite redshift,  $\bar{\kappa}_\infty$  is the unknown constant which represents the average of  $\kappa_\infty$  within the data field  $\mathcal{U}$ ,  $\vec{H}$  is the kernel which is the gradient of the scalar field that satisfies the Neumann boundary problem (see Seitz & Schneider 1996), and  $\vec{u}_{\gamma_\infty} = \hat{D}\gamma_\infty$ . In general, the shear

is not direct observable, so that the integral equation (5) is non-linear and solved iteratively: A mass reconstruction scheme applied to the irregular *HST*/WFC field is outlined in Seitz et al. (1996) and Umetsu, Tada, & Futamase (1999).

In order to determine the constant  $\bar{\kappa}_\infty$ , we employ a dynamical mass estimate of CL 1604+4304 obtained by Postman et al. (1998). Postman et al. (1998) estimated the projected mass inside the circular aperture of radius  $R_{500} = 500h_{50}^{-1}$  kpc at the dynamical center to be  $M_{500} = 0.842 \times 10^{15}h_{50}^{-1}M_\odot$ , corresponding to the mean convergence within the circular aperture of  $\bar{\kappa}_{\infty,500} = M_{500}/\pi R_{500}^2 \Sigma_{\text{cr},\infty} = 0.811$ . However, owing to the small field-of-view of the *HST*/WFPC2, the observed data fields do not cover the whole aperture area even for the 1995 pointing. The effective aperture area covered by the 1995 data field is about 60% of the circular aperture area. We assume that the mean convergence  $\bar{\kappa}_{\infty,\text{eff}}$  inside the effective aperture is the same as the mean convergence  $\bar{\kappa}_{\infty,500}$  inside the circular aperture:  $\bar{\kappa}_{\infty,\text{eff}} \approx \bar{\kappa}_{\infty,500} = 0.811$ . We, thus, solve the integral equation (5) iteratively varying the value of  $\bar{\kappa}_\infty$  in such a way that the average  $\bar{\kappa}_{\infty,\text{eff}}$  of the reconstructed convergence within the effective aperture area equals  $\bar{\kappa}_{\infty,500} = 0.811$ .

### 3.2. Analysis of Cl 1604+4304

Since the 1995 pointing covers the central cluster region where a dynamical analysis was performed by Postman et al. (1998), we first analyzed the 1995 data. We calculated the fields  $\hat{D}\vec{u}_{(\epsilon)}$  with  $\vartheta = 0.4$  ( $150h_{50}^{-1}$  kpc) on  $24 \times 24$  grid points  $\vec{\theta}_{ij}$  (except on the PC chip), from which we obtained the distribution of the weak-lensing S/N within the WFC field. Here we have measured the dispersion  $\sigma_\epsilon$  from the rotation field  $\text{rot}\vec{u}_{(\epsilon)}(\vec{\theta}_{ij})$  in the following way: We calculated the variance  $\sigma_{\text{rot}}^2$  of the noise field  $\text{rot}\vec{u}_{(\epsilon)}(\vec{\theta}_{ij})$  by averaging over the grid points. Equating  $\sigma_{\text{rot}}^2$  with the average of  $\sigma^2(\vec{\theta})$  over the grid points  $\vec{\theta}_{ij}$ , we obtained an estimate of  $\sigma_\epsilon = 0.21$ .

Figure 1 displays the resulting weak-lensing S/N map obtained for the 1995 data. We find two S/N peaks above a threshold of  $\nu_{\text{th}} = 3$ . The first maximum has a peak height of  $\nu = 4.5$  and its location is about  $1.7$  ( $850h_{50}^{-1}$  kpc) southwest of the optical cluster center (marked with cross) determined from the dynamical analysis of Postman et al. (1998). The peak height of the second maximum is  $\nu = 3.6$  and located in the vicinity of the dynamical cluster center. This offset is about  $0.15$  ( $75h_{50}^{-1}$  kpc) and comparable to the grid spacing of  $0.1$  ( $50h_{50}^{-1}$  kpc), so that the second peak is consistent with the dynamical cluster center and associated with the cluster member galaxies (Lubin et al. 1998). In this field, there are a total of 12 cluster members whose redshifts are spectroscopically confirmed by Keck observations (Lubin et al. 1998). However, no cluster members are observed at around the first S/N peak (see Fig. 4 of Lubin et al. 1998) because objects located on the upper edge of the WF4 chip (upper-right WF chip) are not contained within the sampled region of spectroscopic observations (Postman et al. 1998).

Although the detection of the mass concentration cannot be confirmed spectroscopically from the available data, we have checked the stability and reliability of S/N maps.

We find that the main features, i.e. the locations and heights of the peaks, are insensitive to the choice of the weight function or filtering scale. It should be noted that these main features are stable even if objects with large ellipticities ( $|\epsilon| \geq 0.4$ ) are removed from our galaxy catalog, in which case the peak heights of the first and second maxima are 3.7 and 3.0, respectively. There still remains a possibility that the detected S/N peaks might be noise peaks due to the intrinsic source ellipticities or the anisotropic PSF. Van Waerbeke (2000) has shown from the simulated data that the probability distribution of the noise peaks in mass maps deviates from Gaussian and the probability of finding high noise peaks increases owing to the boundary effects. Since the field-of-view of the *HST*/WFC is small and we adopt a constant filtering scale, the obtained S/N maps may be affected by boundary effects. We can investigate such possibilities using independent deep observation of this field. In Fig. 2, we show the weak-lensing S/N map obtained from the 1994 data. Here we have used the same filtering scale and grid spacing as for the 1995 data. Comparing Fig. 2 with Fig. 1, we see that the first maximum in the 1994 S/N map corresponds to that in the 1995 S/N map. The first maximum in the 1994 S/N map has a peak height of  $\nu = 4.2$ , whose location coincides well with that of the first maximum in the 1995 S/N map ( $\alpha_{\text{J2000}} = 16^{\text{h}}04^{\text{m}}15.7^{\text{s}}$  and  $\delta_{\text{J2000}} = +43^\circ 03' 47''.2$ ). The identification of the first S/N maximum from two-different pointing observations indicates that the S/N maximum does not originate from the anisotropic PSF. Moreover, since the first maximum in the 1994 S/N map is located at the center of the WF4 chip, the S/N measure at the first peak cannot be affected by boundary effects. These results confirm the detection of ‘dark’ mass concentration associated with the first S/N maximum.

We have reconstructed the projected mass distribution within the 1995 data field. We calculated the smoothed ellipticity  $\langle \epsilon \rangle(\vec{\theta})$  on  $20 \times 20$  grid points (except on the PC chip) using  $W_G(\theta; \vartheta)$  with  $\vartheta = 0.35$  ( $176h_{50}^{-1}$  kpc). In Fig. 3, we show the reconstructed  $\kappa_\infty$ -map. In mass reconstruction, we implicitly assumed that the dark mass concentration has the same redshift  $z = 0.897$  as Cl 1604+4304. We see from Figs. 1 and 3 that the local maxima in the S/N maps correspond to the mass peaks and that the weak-lensing S/N traces the projected mass, as expected. The  $\kappa_\infty$ -map shows a super-critical feature around the dark mass concentration ( $\kappa_\infty = 1.19$ ) as well as in the cluster central region. The projected mass within the 1995 data field is obtained as  $1.0 \times 10^{15}h_{50}^{-1}M_\odot$ . From the mass map, the enclosed mass in a  $280h_{50}^{-1}$  kpc radius centered on the dark mass concentration is calculated to be  $2.4 \times 10^{14}h_{50}^{-1}M_\odot$ . For the mass-to-light ratio, a lower limit is obtained as  $M/L_B \approx 500h_{50}$  in solar units from an upperlimit on the dark clump’s surface brightness.

## 4. DISCUSSION AND CONCLUSIONS

We have performed a weak-lensing analysis on the deep images of a region around Cl 1604+4304 taken with the *HST*/WFPC2. We detected two significant maxima in the resulting weak-lensing S/N map: the second peak associated with the dynamical cluster center and the first peak located about  $1.7$  south of the dynamical center having no optical counter parts. The identification of high S/N peak

from two-different pointing observations provides a robust evidence of dark mass concentration. Assuming that the dark mass clump has the same redshift as Cl 1604+4304, we reconstructed the projected mass distribution in the 1995 data field, from which we have estimated the mass within a circular aperture of radius  $280h_{50}^{-1}$  kpc centered on the dark clump to be  $2.4 \times 10^{14}h_{50}^{-1}M_{\odot}$ . The obtained results indicate that this dark clump could be a compact, massive bound system associated with the supercluster at  $z \approx 0.9$ ; the obtained mass will be overestimate if the redshift of the dark clump is much less than 0.897.

Our results demonstrate that the weak-lensing S/N statistics are powerful and efficient tools even for high-redshift cluster surveys ( $z \sim 1$ ). For a further confirmation

of the dark mass concentration, deep wide-field observations covering the entire supercluster field ( $\sim 20'$ ) are required. Such observations can probe the mass distribution in the supercluster field extending over  $\sim 10h_{50}^{-1}$  Mpc.

We are very grateful to Toru Yamada, Masahiro Takada, and Masaru Kajisawa for helpful discussions. We thank the anonymous referee for useful comments. Part of this work is based on the observation with the NASA/ESA *Hubble space Telescope*, obtained from the data archive at the Space Telescope Science Institute (STScI). STScI is operated by the Association of Universities for Research in Astronomy, Inc. under the NASA contract NAS 5-26555.

#### REFERENCES

- Bahcall, N. A., Ostriker, J. P., Perlmutter, S., Steinhardt, P. J. 1999, *Sci* 284, 1481B  
 Bartelmann, M. & Schneider, P. 2000, *Phys. Rep.*, submitted  
 Bertin, E. & Arnouts, S. 1996, *A&AS* 117, 393  
 Brainerd, T. G., Blandford, R. D., & Smail, I. 1996 *ApJ*, 466, 623  
 Erben, T., Van Waerbeke, L., Mellier, Y., Schneider, P., Cuillandre, J.-C., Castander, F. J., & Dantel-Fort, M. 2000, *A&A*, 355, 23  
 Kaiser 1995, *ApJ*, 439, L1  
 Kaiser, N. & Squires, G. 1993, *ApJ*, 404, 441  
 Kaiser, N., Wilson, G., Luppino, G., Kofman, L., Gioia, I., Metzger, M., & Dahle, H. 1998, preprint astro-ph/9809268  
 Lubin, L., Postman, M., Oke, J. B., Ratnatunga, K. U., Gunn, J. E., Hoessel, J. G., & Schneider D. P. 1998, *ApJ*, 116, 584  
 Lubin, L., Brunner, R., Metzger, M. R., Postman, M., Oke, J. B., 2000, *ApJ*, 531, L5  
 Luppino, G. A. & Kaiser, N. 1997, *ApJ*, 475, 20  
 Oke, J. B., Postman, M., & Lubin, L. 1998, *ApJ*, 116, 549  
 Postman, M., Lubin, L., & Oke, J. B. 1998, *ApJ*, 116, 560  
 Schneider, P. 1996, *MNRAS*, 283, 837  
 Seitz, C. Kneib, J.-P., Schneider, P., & Seitz, S. 1996, *A&A*, 314, 707  
 Seitz, S. & Schneider, P. 1996, *A&A*, 305, 383  
 Seitz, C. & Schneider, P. 1997, *A&A*, 318, 687  
 Umetsu, K., Tada, M., & Futamase, T. 1999, *Prog. Theor. Phys. Suppl.*, 133, 53  
 Van Waerbeke, L. 2000, *MNRAS*, 313, 524

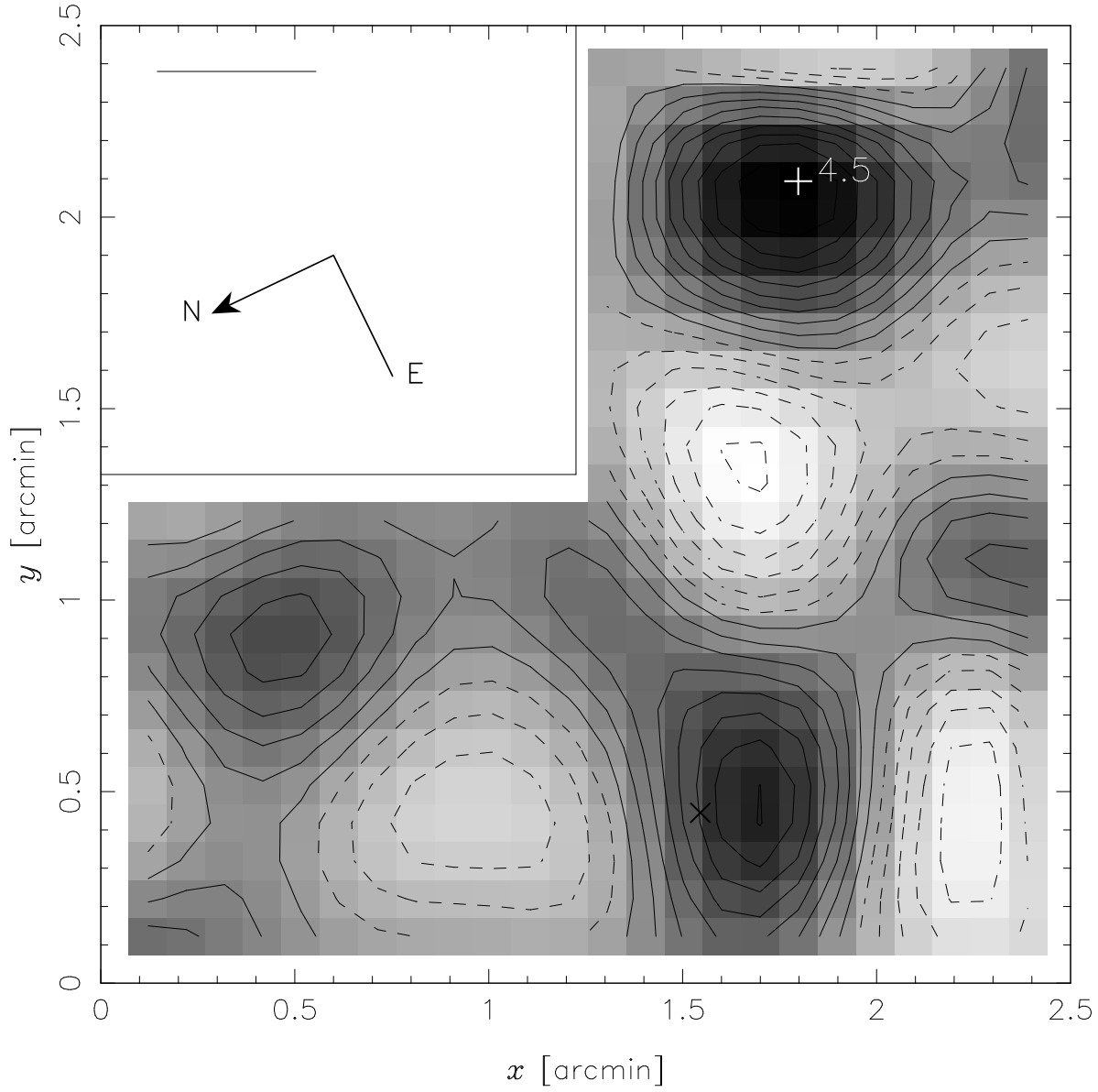


FIG. 1.— Contour plot of the weak-lensing signal-to-noise ratio distribution obtained from 241 galaxy images with  $I_{814W} \in (25.5, 27.5)$  taken with the *HST*/WFPC2 in 1995. The solid and dashed lines indicate the positive and negative ones, respectively. The contours are stepped in units of 0.5. The filtering scale ( $0''.4$ ) used for the aperture mass measure is marked and the position of the dynamical cluster center is indicated ( $\times$ ). The location of the first maximum is marked with  $+$ . The peak height of the second maximum is 3.6 and its location coincides well with the dynamical center.

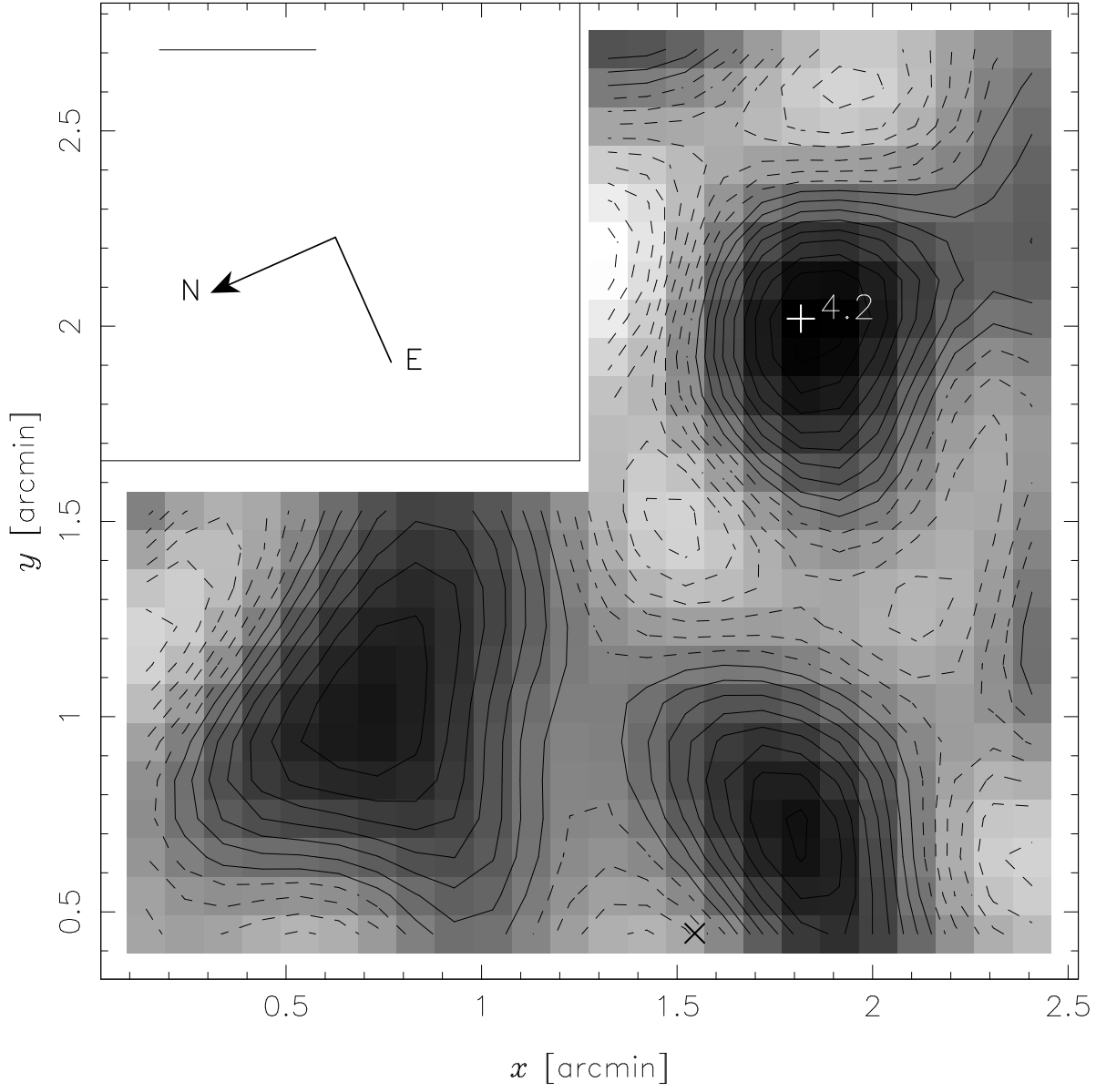


FIG. 2.— The same as Fig. 1 but obtained from 200 galaxy images with  $I_{814W} \in (25.5, 27.5)$  taken with the *HST*/WFPC2 in 1994. The same coordinate system as in Fig. 1 is used.

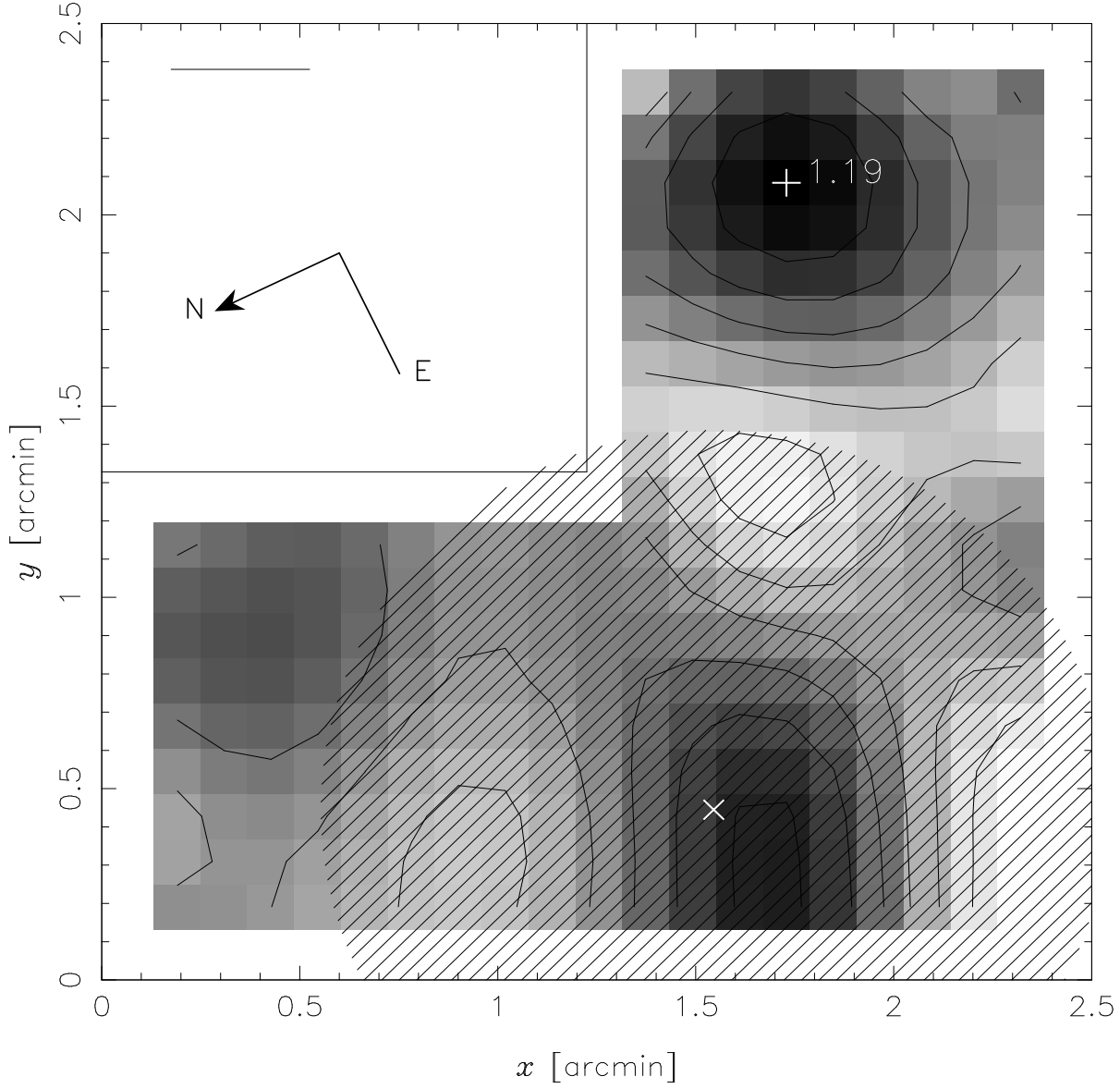


FIG. 3.— Contour plot of the  $\kappa_\infty$ -distribution reconstructed from the shear field of the 1995 observation. The contours are stepped in units of 0.1. The smoothing scale ( $0''.35$ ) used to calculate the shear field is marked. The shaded area indicates the circular aperture of radius  $500h_{50}^{-1}$  kpc centered on the dynamical cluster center (marked with  $\times$ ). The side length is about  $2''.5$  ( $1.26h_{50}^{-1}$  Mpc at  $z = 0.897$ ). The mass distribution is super-critical around the first maximum (marked with  $+$ ) and the cluster central region.